Crystallographic Analyses of Site-Directed Mutants of the Photosynthetic Reaction Center from *Rhodobacter sphaeroides*[†,‡]

Arthur J. Chirino,[▽,§] Erik J. Lous,[∥,⊥] Martina Huber,[∥,#] James P. Allen,[△] Craig C. Schenck,[∞] Mark L. Paddock,[∥] George Feher,[∥] and Douglas C. Rees*[,▽]

Division of Chemistry and Chemical Engineering 147-75CH, California Institute of Technology, Pasadena, California 91125, Department of Physics, University of California at San Diego, La Jolla, California 92093, Deparment of Chemistry and Biochemistry, Arizona State University, Tempe, Arizona 85827, and Department of Biochemistry, Colorado State University, Fort Collins, Colorado 80523

Received September 21, 1993; Revised Manuscript Received February 7, 1994[⊛]

ABSTRACT: Seven site-directed mutants of the bacterial photosynthetic reaction center (RC) from the 2.4.1 and WS 231 wild-type strains of *Rhodobacter sphaeroides* have been crystallized and their X-ray diffraction analyzed to resolutions between 3.0 and 4.0 Å. The mutations can be divided into four distinct categories: (1) mutations altering cofactor composition that affect electron transfer and quantum yield, His M202 → Leu (M202HL), His L173 → Leu (L173HL), and Leu M214 → His (M214LH); (2) a mutation in the proposed pathway of electron transfer altering electron-transfer kinetics, Tyr M210 → Phe (M210YF); (3) a mutation around the non-heme iron resulting in an iron-less reaction center, His M219 → Cys (M219HC); and (4) mutations around the secondary electron acceptor, a ubiquinone, affecting proton transfer and quinone turnover, Glu L212 → Gln (L212EQ) and Asp L213 → Asn (L213DN). Residues L173 and M202 are within bonding distance of the respective magnesiums of the two bacteriochlorophylls of the BChl special pair, while M214 is close to the bacteriopheophytin on the active A branch of the RC. The L173HL and M202HL crystal structures show that the respective bacteriochlorophylls are replaced with bacteriopheophytins (i.e., loss of magnesium) without significant structural perturbations to the surrounding main-chain or side-chain atoms. In the M214LH mutant, the bacteriopheophytin has been replaced by a bacteriochlorophyll, and the side chain of His M214 is within ligand distance of the magnesium. The M210YF, L212EQ, and L213DN mutants show no significant tertiary structure changes near the mutation sites. The M219HC diffraction data indicate that the overall tertiary structure of the reaction center is maintained in the absence of the non-heme iron.

The bacterial photosynthetic reaction center (RC[1]) is an integral membrane protein that mediates charge separation across the membrane during the initial steps of photosynthesis. The RC serves as a paradigm for understanding electron transfer, since extensive biochemical, spectroscopic, and kinetic data have been compiled on this system, and crystal structures of RCs from two species of purple bacteria, *Rhodopseudomonas* (*Rps.*) *viridis* and *Rhodobacter* (*Rb.*) *sphaeroides*, have been determined to near-atomic resolution (Deisenhofer et al., 1985; Allen et al., 1987; Chang et al., 1991; Ermler et al., 1992), allowing extensive theoretical examination (Michel-Beyerle et al., 1988; Warshel et al., 1989; Parson et al., 1990; Treutlein et al., 1992). RCs isolated from wild-type strains of *Rb. sphaeroides* contain three membrane-spanning protein subunits (L, M, and H) and ten cofactors (four type *a* bacteriochlorophylls, two *a* bacteriopheophytins, two ubiquinones, one non-heme iron, and one carotenoid). The RC crystal structure shows that the L and M subunits and the cofactors are structurally related to each other by an approximately 180° rotation. Electron transfer in the RC proceeds along a series of cofactors: from the primary donor (D), a bacteriochlorophyll dimer, to an intermediate acceptor (BPh_A), a bacteriophenophytin, to the primary acceptor (Q_A), a ubiquinone, and finally to the secondary electron acceptor (Q_B), also a ubiquinone [reviewed in Feher et al. (1989)]. Concomitant with the two-electron reduction of Q_B, two protons are picked up to form Q_BH_2, which dissociates from the RC and is subsequently replaced by an exogenous quinone (McPherson et al., 1990a). Due to the similar structural arrangement of cofactors in the two branches, two-electron-transfer pathways are potentially available. Strikingly, electron transfer predominantly occurs along only one branch. This behavior must be due to different cofactor–protein interactions along the two branches (Deisenhofer et al., 1985;

[†] This work was supported by the National Institutes of Health (GM45162 to D.C.R., GM41300 to J.P.A., GM13191 to G. F., GM41637 to M.L.P., and R.C.D.A. GM00536 and GM38214/48254 to C.C.S.). E.J.L. was supported by the European Molecular Biology Organisation and M.H. by a Forschungsstipendium of the Deutsche Forschungsgemeinschaft.

[‡] Refined coordinates for the 2.4.1 wild-type RC and the M202HL mutant RC structures have been deposited in the Brookhaven Protein Data Bank under file names 1PSS and 1PST, respectively.

* Author to whom correspondence should be addressed. Telephone: (818)395-8393. FAX: (818)568-9430. e-mail: REES@CITRAY.CALTECH.EDU.

[▽] California Institute of Technology.

[§] Current address: Department of Molecular Biophysics and Biochemistry, Yale University, New Haven, CT 06511.

[∥] University of California at San Diego.

[⊥] Current address: Department of Experimental Physics, Philips Research Laboratories, P.O. Box 80000, 5600 JA Eindhoven, The Netherlands.

[#] Current address: Institut für Organische Chemie, Freie Universität Berlin, Takustrasse 3, D-14195, Berlin, Germany.

[△] Arizona State University.

[∞] Colorado State University.

[⊛] Abstract published in *Advance ACS Abstracts*, March 15, 1994.

[1] Abbreviations: RC, bacterial photosynthetic reaction center; *Rb.*, *Rhodobacter*; *Rps.*, *Rhodopseudomonas*; BChl, bacteriochlorophyll; BPh, bacteripheophytin; D, primary donor; $|F_o|$, observed structure factor amplitudes; $|F_c|$, calculated structure factor amplitudes; SA, simulated annealing/molecular dynamics refinement.

0006-2960/94/0433-4584$04.50/0

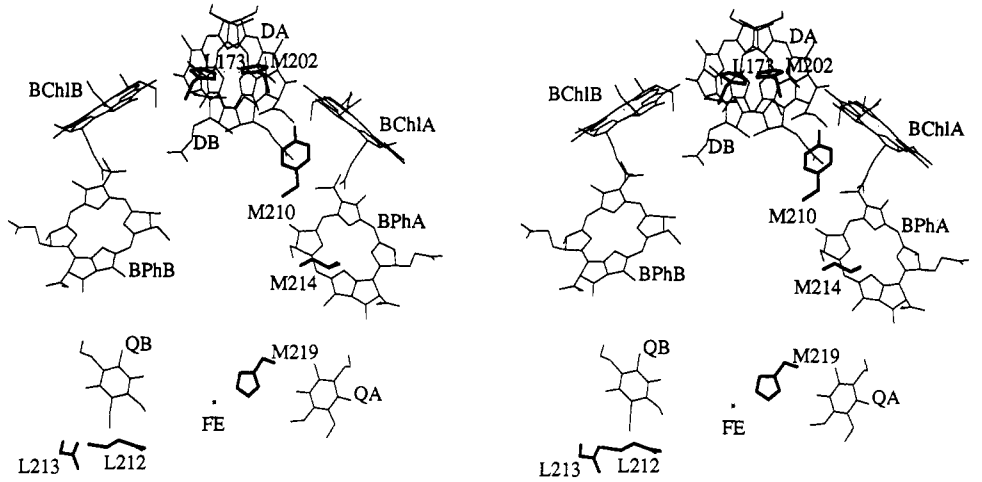

FIGURE 1: Stereoview of the RC cofactors (except carotenoid) from the 2.4.1 strain of *Rb. sphaeroides*. Residues of the native sequence that have been mutated in the current study are outlined in bold type.

Komiya et al., 1988; Michel-Beyerle et al., 1988; El-Kabbani et al., 1991).

Site-directed mutagenesis is a powerful tool for investigating these cofactor–protein interactions, as well as structure–function relationships in general. Mutagenesis protocols have been available for some time for RCs from *Rb. capsulatus* (Youvan et al., 1985) and *Rb. sphaeroides* (Farchaus & Oesterhelt, 1989; Paddock et al., 1989; Takahashi et al., 1989; Hammes et al., 1990). Production of RC mutants in these bacteria is facilitated by the ability of the organisms to grow nonphotosynthetically while still expressing RC (Yen & Marrs, 1977); this eliminates the selective pressure of nonfunctioning mutant RCs to revert back to the wild type. Since the structure of *Rb. capsulatus* has not yet been determined and *Rps. viridis* is only able to grow photosynthetically (Laussermair & Oesterhelt, 1992), *Rb. sphaeroides* represents, at present, the system of choice to examine both functional and structural changes due to the mutations.

Site-directed mutagenesis has been used to create a series of mutant RCs from *Rb. sphaeroides* to probe the function of certain residues that, judging from the crystal structure, were logical targets due to their proximity to cofactors and to sequence conservation among bacterial and algal RCs (Komiya et al., 1988). The altered functional behavior of a given mutant may be due to the difference in chemical nature of the residue substitution, a structural change in the protein, or both. To distinguish these two effects, the crystal structures of the mutant RCs have been determined. The known characteristics of the seven site-directed mutants examined in this report are briefly described here (see Figure 1). The structure and functional behavior of other types of modified RCs (e.g., removal of the secondary quinone and binding of herbicides) have been discussed elsewhere (Allen et al., 1990).

BIOCHEMICAL, SPECTROSCOPIC, AND KINETIC CHARACTERISTICS OF THE MUTANTS

Donor-Modifying Mutants: His L173 → Leu (L173HL) and His M202 → Leu (M202HL). Spectroscopic and kinetic evidence suggest that one bacteriochlorophyll of the special pair dimer, D_A or D_B, is replaced by bacteriopheophytin when either histidine L173 or M202 (M200 in *Rb. capsulatus*) is replaced by a leucine to form the L173HL and M202HL mutants, respectively[2] (Bylina & Youvan, 1988; Kirmaier et al., 1988; McDowell et al., 1991). This results in the formation of a dimer composed of a BChl–BPh pair called a "heterodimer" that is still capable of electron transfer. Electron transfer remains unidirectional along the A branch in the M202HL and L173HL mutants, but the quantum yield for the formation of $D^+ \cdot BPh_A^-$ is reduced from nearly 1.0 in wild-type RC to ~0.5, due to a decrease in the forward reaction rate from $D \cdot BPh_A$ to $D^+ \cdot BPh_A^-$ as well as an increase in the recombination rate to the ground state (McDowell et al., 1991). The unpaired electron (hole) on D^+ is localized on the BChl half of the dimer, whereas in the wild-type RC it is delocalized over the entire dimer [reviewed in Feher (1992)].

Bacteriopheophytin-Modifying Mutant: Leu M214 → His Mutant (M214LH). After photoexcitation of the primary donor, the $D^+ \cdot BPh_A^-$ state in wild-type RCs is formed in ~3 ps. Leucine M214 is located near BPh_A in the wild-type *Rb. sphaeroides* RC. Substitution of this residue by histidine in the M214LH mutant is associated with the replacement of BPh by BChl (Kirmaier et al., 1991); it was therefore assumed that this histidine is liganded to the Mg. The M214LH mutant exhibits an electron-transfer rate between D and BPh_A of ~6 ps (half as fast as the wild type) with a quantum efficiency of 0.6 in producing $D^+Q_A^-$ (Kirmaier et al., 1991). Despite the considerably higher midpoint redox potential for the reduction of BPh as compared to BChl, only a small change in the energy of the intermediate electron acceptor is detected by time-resolved fluorescence (Kirmaier et al., 1991). This suggests that any intrinsic changes in redox potential associated with the substitution of BChl for BPh may be compensated by associated structural changes.

Electron-Transfer Mutant: Tyr M210 → Phe (M210YF). Tyrosine M210 in the native 2.4.1 RC is positioned near four porphyrin ring structures (D_A, D_B, $BChl_A$, and BPh_A) and is conserved in most of the bacterial and algal RC protein sequences (Komiya et al., 1988). The tyrosine hydroxyl group of M210 is approximately 3.6 Å from the oxygen of the ring IV propionic acid carbonyl of D_A and 4.0 Å from the acetyl oxygen of ring I of D_B in 2.4.1 RC and may be involved in electrostatic interactions (see Results and Discussion). The M210YF mutant exhibits electron-transfer properties altered from those of the wild-type RC; the electron-transfer rate of

[2] Mutated residues are designated in this article by the nomenclature, (subunit) (residue number) (wild-type amino acid) (substituted amino acid), i.e., L173HL represents the substitution of histidine by leucine at residue 173 of the L subunit.

$D{\cdot}BPh_A \rightarrow D^+{\cdot}BPh_A^-$ decreases by approximately a factor of 5 (Finkele et al., 1990; Nagarajan et al., 1990, 1993; Jia et al., 1993).

Non-Heme Iron Mutant: His M219 → Cys (M219HC). The non-heme iron (Fe^{2+}) is six-coordinated to five protein side chains (histidines L190, L230, M219, and M266 and glutamate L234) and lies between the primary and secondary acceptors Q_A and Q_B (Allen et al., 1988). Since the iron can be replaced by several other divalent cations such as Cu^{2+}, Co^{2+}, and Ni^{2+} without affecting the electron-transfer kinetics between the quinones (Debus et al., 1986), the role of the non-heme iron (or other substituted divalent cation) was thought to lend structural stability to the RC. The M219HC mutant has been shown to be devoid of iron and several other divalent metals (Williams et al., 1991), yet crystals isomorphous to native RC were obtained. These mutants display altered $D^+{\cdot}Q_A^-{\cdot}Q_B \rightarrow D^+{\cdot}Q_A{\cdot}Q_B^-$ kinetics that are similar to those exhibited by RCs depleted of divalent metals (Williams et al., 1991).

Proton-Transfer Mutants: Glu L212 → Gln (L212EQ) and Asp L213 → Asn (L213DN). Following the two-electron reduction of the secondary quinone, Q_B picks up two protons from the solvent on the cytoplasmic side of the bacterial membrane and dissociates from the RC (McPherson et al., 1990a). This process initiates the creation of a proton gradient across the membrane. Since the head group of Q_B is located ~10 Å from any solvent-exposed surface (Allen et al., 1988), a proton-transfer mechanism involving intervening protonatable residues participating in a charge-relay system has been postulated [reviewed in Okamura and Feher (1992)]. Several ionizable side chains lie within 5.0 Å of Q_B and are potential candidates for direct cofactor protonation. Still other ionizable side chains line a potential pathway toward the solvent region (Allen et al., 1988). Glutamate L212 and aspartate L213 are ionizable groups within 5.0 Å of the Q_B ring that are likely to be involved in quinone protonation and have therefore been the subject of a number of mutagenesis experiments (Paddock et al., 1989; Takahashi & Wraight, 1992).

The L212EQ mutant RC displays wild-type $Q_A^-{\cdot}Q_B \rightarrow Q_A{\cdot}Q_B^-$ electron-transfer rates for pH < 8. The rates in the mutant are pH-independent, in contrast to the wild-type RC in which the rate decreases drastically at pH > 8 (Paddock et al., 1989). The proton uptake rate displays a slow phase, which limits the rate of formation of Q_BH_2 (McPherson et al., 1990b). This suggests the involvement of L212 in the second protonation step of Q_B. Since the distance between L212 and the carbonyl oxygen of Q_B is too large to form a hydrogen bond (Allen et al., 1988), direct or indirect protonation by L212 would require either the involvement of buried water molecules, hydrogen tunnelling, or movement of either Q_B or the L212 side chain following the reduction of Q_B. While the crystallographic analysis of L212EQ cannot distinguish between L212's direct or indirect involvement in a protonation mechanism or whether movement is a prerequisite for protonation, it can detect major changes in the three-dimensional structure of the mutant, which would complicate the explanation of the mutant's electron-proton-transfer behavior.

In contrast to the L212EQ mutation, substitution of Asp L213 to Asn (L213DN) exhibits a decrease of ~6000-fold in the electron-transfer and proton uptake rates associated with the second electron reduction of Q_B ($Q_A^-Q_B^- + 2H^+ \rightarrow Q_AQ_BH_2$). Intriguingly, substitution of Asn M44 by Asp restores the photosynthetic viability of the L213DN mutant (Okamura et al., 1992; Rongey et al., 1993; Hanson et al., 1992, 1993), indicating that the proton-coupled electron-transfer reaction associated with the second reduction step of Q_B is accelerated by the presence of negatively charged Asp residues near Q_B. In the structural model for the proton-transfer pathway described by Okamura and Feher (1992), Asp L213 participates in pathways for both the first and second proton transfers. Given the significance of L213 in proton transfer, crystallographic analysis of the L213DN mutant should help assess the structural consequences of this substitution.

EXPERIMENTAL PROCEDURES

Site-Directed Mutagenesis, Crystallization, and Data Collection. Site-directed reaction center mutants from wild-type strains of *Rb. sphaeroides* (2.4.1 and WS 231) were prepared as previously described (Paddock et al., 1989; Hammes et al., 1990). Crystals of mutant RCs were grown under conditions similar to those used to crystallize native RCs from 2.4.1 and R-26 strains of *Rb. sphaeroides* (Allen et al., 1986, 1988). The crystals of the mutant reaction centers were found to be isomorphous to the native ones (space group $P2_12_12_1$ with cell dimensions a = 138.0 Å, b = 77.5 Å, and c = 141.8 Å), with maximal deviations of cell constants from the native values of <0.5% (with the exception of the M219HC mutant RC, which had cell dimensions a = 136.0 Å, b = 76.9 Å, and c = 142.4 Å). Crystals typically measured 0.6 × 0.6 × 4.0 mm, although smaller and more weakly diffracting crystals were obtained from some mutants.

Diffraction data from native 2.4.1, M202HL, L173HL, L213DN, M210YF, and M219HC mutant RCs were collected using a Siemens X-100 area detector with a three-circle goniometer mounted on a Siemens rotating anode generator operating at 50 kV × 90 mA. Monochromatic Cu K_α radiation (λ = 1.5418 Å) was used throughout the data collection. All data were processed with the XENGEN (version 1.3) data reduction package (Howard et al., 1987). The final reduced data set for each structure was collected from one crystal. For use in difference Fourier maps, reduced data sets were locally scaled (Matthews & Czerwinski, 1975) to the native 2.4.1 RC data, using the ROCKS crystallographic package (Reeke, 1984; Bethge, 1984). The native 2.4.1 RC diffraction data used for the work reported in this article were collected independently from those described in Yeates et al. (1988).

Diffraction data of L212EQ and M214LH mutant RC crystals were collected on a Hamlin–Xoung two-panel multiwire area detector system (Hamlin, 1985), with a Huber four-circle goniometer mounted on a Rigaku RU-200 rotating anode generator operating at 50 kV × 90 mA. Monochromatic Cu K_α radiation (λ = 1.5418 Å) was also used throughout the data collection. San Diego Area detector software (Howard et al., 1985) was used during data collection. The observations were merged and the data scaled with the DIFCOR program in the ROCKS crystallographic package (Reeke, 1984; Bethge, 1984). The final reduced data set for each mutant was collected from one crystal.

Data collection statistics for the various data sets described in this article are summarized in Table 1.

Crystallographic Analysis, Refinement, and Model Building. The initial analysis of each mutant included the examination of difference Fourier electron density maps calculated with ($|F_o$(native)$| - |F_o$(mutant)$|$) or ($|F_o$(mutant)$| - |F_c$(native)$|$) coefficients, with model amplitudes and phases calculated from the current 2.4.1 RC coordinates (see Results and Discussion). Crystallographic refinement was performed using the X-PLOR refinement package (Brünger et al., 1987). Structural refinement was only carried out on a mutant if crystals of that mutant diffracted to at least 3.0-Å resolution (see Table 1). Refinement of a mutant began with the current

Table 1: Reaction Center Data Collection Statistics[a]

data set	resolution (Å)	observed reflections	unique reflections	% complete	R, merge	R, native
2.4.1	3.0	61 853	21 518	68.9	0.077	
M202HL	3.0	67 299	22 184	71.1	0.103	0.125
L173HL	4.0	33 232	16 262	67.7	0.161	0.169
M210YF	3.0	67 214	20 085	64.3	0.145	0.134
M214LH	3.3	89 230	16 934	67.8	0.132	0.189
M219HC	4.0	35 457	6 894	51.2	0.221	0.383
L212EQ	3.3	100 308	19 780	75.4	0.132	0.146
L213DN	3.0	75 566	23 261	74.5	0.078	0.100

[a] Resolution indicates the limiting resolution used in the collection of a particular data set, while % complete indicates the fraction of possible reflections to the limiting resolution actually present in the merged data set (with $|F_O| > 0$ for all data sets, except for M214LH and L212EQ, for which $|F_O| > \sigma_F$). R, merge, is defined as $\sum_{hkl}\sum_i|I_{hkl,i} - \langle I_{hkl}\rangle|/\sum_{hkl}\sum_i I_{hkl,i}$, while R, native, between the mutant and native data sets is defined as $\sum_{hkl}||F_{mutant}| - |F_{native}||/\sum_{hkl}|F_{native}|$, calculated between 8- and 5-Å resolution.

native 2.4.1 RC coordinates. The native model consisted of residues 5-270 of subunit L, 6-301 of M, 12-248 of H, and the 10 cofactors (D_A, D_B, $BChl_A$, $BChl_B$, BPh_A, BPh_B, Q_A, Fe, Q_B, and sphaeroidene). Rigid body refinement in X-PLOR was used to compensate for slight changes in RC packing. Typical rounds of molecular dynamics/simulated annealing refinement included the standard slow-cool protocol (Brünger et al., 1990), followed by 120 steps of conjugate gradient least-squares minimization, a maximum of 15 steps of overall isotropic temperature factor refinement, and 20 steps of tightly restrained individual atomic temperature factor refinement. Omit–refine maps ($|F_o| - |F_c|$) were calculated by first removing the residue of interest and the surrounding 1–2 residues on either side and then subjecting the modified model to 100 cycles of conjugate gradient least-squares minimization in X-PLOR. Interactive model building was performed using a version of the TOM/FRODO program for Silicon Graphics Iris workstations (Jones, 1985) that was locally modified by A.J.C. to include interactive fragment fitting and rotamer libraries. Least-squares superposition of refined mutant models onto the 2.4.1 model was performed using the algorithm of Kabsch (1976). Refined coordinates for the 2.4.1 wild-type RC and the M202HL mutant RC structures have been deposited in the Brookhaven Protein Data Bank.

RESULTS AND DISCUSSION

Refinement of the RC from the Wild-Type 2.4.1 Strain of Rb. sphaeroides. The crystallographic analyses of the mutant RCs were based on comparisons to the native 2.4.1 RC structure. The refined 2.8-Å resolution R-26 RC crystal structure[3] (Yeates et al., 1988) was used as the starting point for the 2.4.1 structure refinement. Diffraction data of 2.4.1 RC crystals were collected to 3.0-Å resolution (Table 1). After rigid body refinement of the R-26 model against the 2.4.1 data, the sphaeroidene carotenoid cofactor was built into the $|F_o| - |F_c|$ difference electron density. Using models without carotenoid from subsequent rounds of least-squares refinement in difference map calculations improved the quality of the carotenoid difference density. The 2.4.1 RC model was subjected to SA refinement using all non-zero reflections between 8.0 and 3.0 Å (19 780 reflections). The free R factor (Brünger, 1992) decreased throughout refinement, demonstrating that useful changes were being made to the structure. The current R value is 0.223 ($|F| > 2\sigma_F$(18 066 reflections), RMS_{bond} = 0.013 Å, and RMS_{angle} = 3.4°).

[3] Entry 4RCR in the Brookhaven Protein Data Bank (Bernstein et al., 1977).

Table 2: Magnesium–Histidine Nε2 Distances (Å) in the Special Pair of Bacterial RCs[a]

residue	R-26[b]	2.4.1[c]	R-26[d]	2.4.1[e]	M202HL[f]	M210YF[g]	*Rps. viridis*[h]
L173 D_A	2.7	2.6	3.2	2.6	2.7	3.0	2.2
M202 D_B	2.2	2.1	2.2	2.7	NA	2.0	1.9

[a] On the basis of small-molecule structures, Mg–N distances of ~2.0–2.1 Å would be expected for a liganding interaction in a five-coordinate Mg–porphyrin complex (Chow et al., 1975; Yang & Jacobson, 1991). [b] PDB data set 4RCR. [c] This work (PDB data set 1PSS). The estimated coordinate error is ~0.5 Å. [d] PDB data set 2RCR (Chang et al., 1991). [e] Ermler et al. (1992). [f] This work (PDB data set 1PST). [g] This work (coordinates not deposited in the PDB). [h] PDB data set 1PRC (Deisenhofer et al., 1985).

The most significant difference between the refined 2.4.1 RC structure and the R-26 model previously described by our group (Yeates et al., 1988) is in the coordination of the bacteriochlorophyll by histidines. In the wild-type RC, histidines L173 and M202 are located near each BChl of the special pair dimer and are poised to act as ligands to the central porphyrin magnesiums (Table 2). The side chains of histidines L153 and M182 are near the magnesiums of the monomeric bacteriochlorophylls. In the earlier R-26 RC structure, the Nε2 atoms of the His L173 and L153 side chains were too far from the adjacent BChl magnesiums (~4 Å) to serve as ligands, while the Nε2 atoms of histidines M202 and M182 were separated from the adjacent magnesiums by a more typical distance of ~2 Å. Further refinement of the R-26 RC structure (D. C. Rees et al., unpublished results), prior to coordinate deposition in the Brookhaven Protein Data Bank (entry 4RCR), resulted in a decrease in the His L173–Mg distance to 2.7 Å, although no change in the His L153–Mg interaction was indicated. In the present work, the four histidine side chains adjacent to the bacteriochlorophylls were reexamined in the 2.4.1 RC structure. To avoid possible steric clash between the Nε2-H of the histidines and the Mg's of the bacteriochlorophylls, these side chains were SA-refined as singly protonated groups (i.e., with the Nε2 atoms deprotonated). Following refinement, more normal Nε2–Mg distances were observed (ca. <3 Å) for all four histidine–Mg pairs in the 2.4.1 RC structure, suggesting that the earlier values reported for the R-26 RC structure were too high.

Whether histidines L173 and M202 are true ligands to the magnesiums of the special pair has been a matter of some discussion (Deisenhofer et al., 1985; Yeates et al., 1988; Chang et al., 1991; Ermler et al., 1992). In small-molecule structures of chlorophyll derivatives with five-coordinate magnesium, magnesium–water oxygen and magnesium–pyrrole nitrogen distances of ~2.0–2.1 Å are observed (Chow et al., 1975; Yang & Jacobson, 1991); the magnesium–histidine nitrogen coordination distances should be similar. In the 2.3-Å resolution structure of the *Rps. viridis* RC[4] (Michel et al., 1986), both histidines (L173 and M200) act as ligands to the primary donor bacteriochlorophyll magnesiums (distances ~2.0 Å). However, in RCs from *Rb. sphaeroides*, consistently longer histidine–magnesium distances have been observed, with Mg–N distances of 2.2–2.7 Å for His M202 (on the D_B half) and 2.6–3.2 Å for His L173 (on the D_A half) having been reported (Table 2). The consistently larger values for the Mg–histidine distances in the *Rb. sphaeroides* RC, relative to the *Rps. viridis* RC, suggest that the former structure has weaker Mg–histidine bonds compared to the latter, especially for His L173, although the lower resolution of the *Rb.*

[4] Entry 1PRC in the Brookhaven Protein Data Bank (Bernstein et al., 1977).

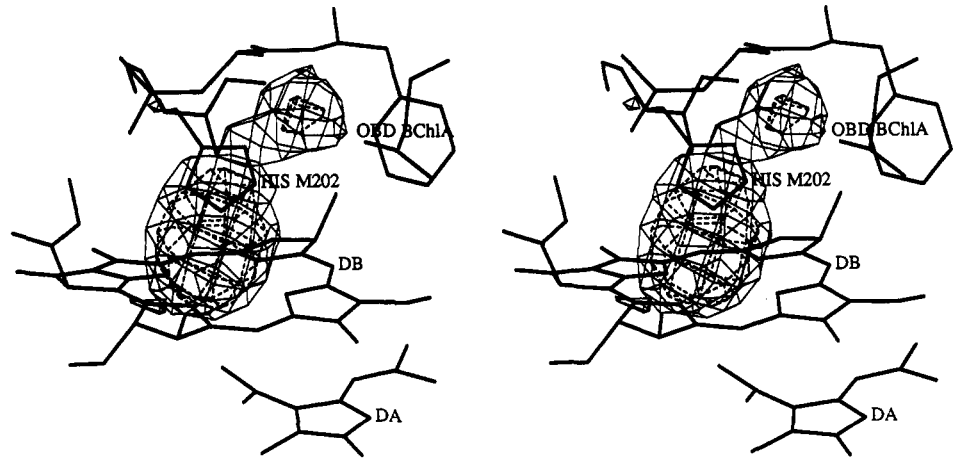

FIGURE 2: Stereo image of a difference Fourier electron density map around the M202 site using ($|F_o(2.4.1)| - |F_o(M202HL)|$) coefficients calculated between 20- and 3.0-Å resolution. All atoms from the 2.4.1 structure within 15.0 Å of M202 C_α are shown. Contour levels are shown at $+3.0\sigma$ (dashed lines) and $+5.0\sigma$ (thin lines), where 1.0σ is the average fluctuation of difference density throughout the unit cell. The main difference density peak is due to the substitution of leucine for histidine and the loss of Mg; the secondary difference peak is located at a site that is occupied by a water molecule in the *Rps. viridis* RC structure.

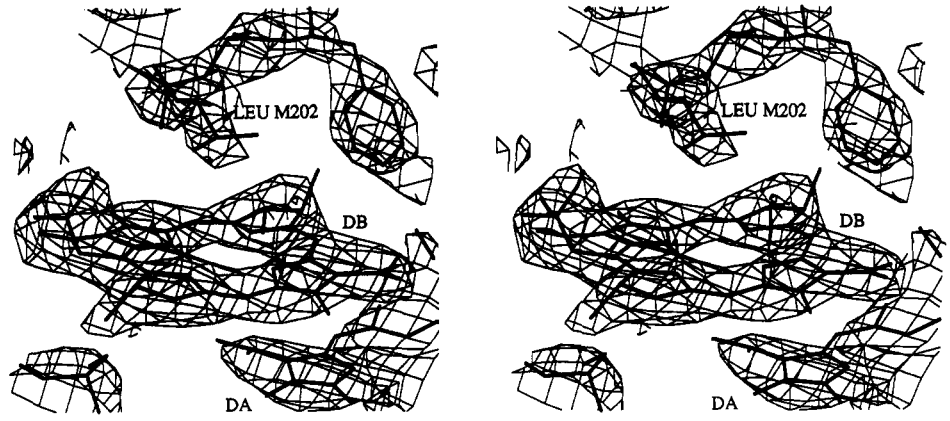

FIGURE 3: Stereo image of a ($2|F_o$(M202HL)| - $|F_c$(M202HL, refined model)|) electron density map calculated between 8.0- and 3.0-Å resolution, within a 12 × 12 × 12 Å box around residue M202. The map is contoured at $+1.5\sigma$. Note the loss of density at the center of the porphyrin ring.

sphaeroides RC structures and the corresponding greater coordinate uncertainty relative to the *Rps. viridis* RC structure make it difficult to assess the statistical significance of these differences in Mg–ligand distances. Whether this apparent difference between the *Rb. sphaeroides* and *Rps. viridis* Mg coordination geometry has any functional consequences is unclear. It should be emphasized that these structures correspond to the neutral, ground state of the RC; it is possible that changes in these ligation interactions can accompany formation of the photoexcited and/or subsequently formed charge-separated intermediate states.

Donor-Modifying Mutants: His L173 → Leu (L173H) and His M202 → Leu (M202HL). Following refinement of the native 2.4.1 structure, difference Fourier maps with coefficients ($|F_o(2.4.1)| - |F_o(M202HL)|$) and model phases from the native 2.4.1 RC model were calculated at 3.0-Å resolution. The positive difference density illustrated in Figure 2 (with a peak maximum of $+10.5\sigma$, the largest in the crystallographic asymmetric unit) extends from the middle of the histidine side chain of M202 to the center of the D_B porphyrin ring as a result of the side chain and cofactor substitutions. The centroid of this density is located directly between the side chain and the porphyrin ring, coinciding with the distribution center of missing electrons, where the distribution comprises ~10 electrons due to the histidine to leucine substitution and 10 electrons due to the loss of Mg^{2+}.

The second largest positive difference peak ($+5.6\sigma$) is located ~3.0 Å from the histidine Nδ1 position of M202 in 2.4.1 RC and the keto carbonyl oxygen of ring V of $BChl_A$ (designated as atom OBD). This site is occupied by a water molecule in the 2.3-Å resolution *Rps. viridis* RC structure, and the difference map suggests that there is also a water molecule at this location in the native 2.4.1 RC. Refinement of the 2.4.1 model with a water oxygen at this site was performed, but the resulting isotropic temperature factor of the water was greater than 80.0 $Å^2$. Although the electron density peak height corresponding to this proposed water is as high as the side-chain difference peak, suggesting that the site is fully occupied by water in the native structure, the resolution of the 2.4.1 RC diffraction data is apparently insufficient to accurately refine waters.

After replacement of the histidine side chain of M202 with leucine and the bacteriochlorophyll (D_B) with a bacteriopheophytin, the 2.4.1 model coordinates were refined against the M202HL data. Rigid body refinement using reflections between 8.0 and 5.0 Å (4913 reflections) decreased the R factor from 0.307 to 0.299; the largest movement was a 0.3-Å translation along the b unit cell axis. SA refinement using reflections between 8.0 and 3.0 Å (20 448 reflections) reduced the R value to 0.218 [$|F| > 2\sigma_F$ (17 962 reflections), RMS_{bond} = 0.013 Å, and RMS_{angle} = 3.4°]. Electron density maps calculated with ($2|F_o| - |F_c|$) coefficients around the mutation site using refined M202HL model phases show excellent

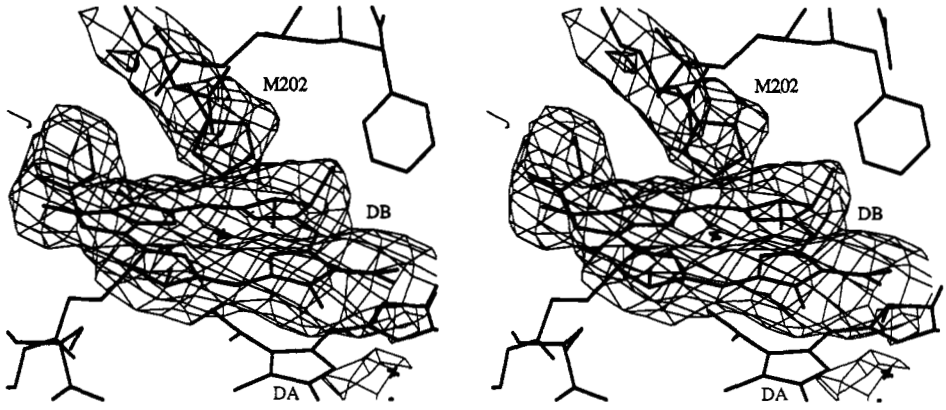

FIGURE 4: Stereo image of an ($|F_o(2.4.1) - |F_c(2.4.1, refined model)|$) electron density map around the M202 site with the same view as Figure 3 ($+2.5\sigma$) for comparison. Residues M201–M203 and D_B were omitted from the calculation of F_c. The contours follow the His M202 residue and the porphyrin ring of D_B.

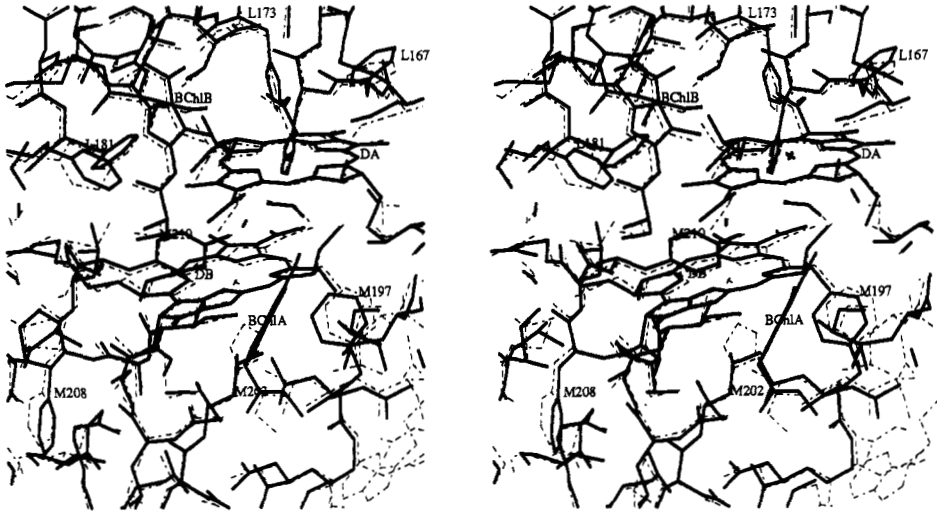

FIGURE 5: Stereoview of the least-squares superposition of the M202HL refined model (solid lines) on the native 2.4.1 model (dashed lines) of atoms within ~10 Å of the special pair cofactors. The maximum absolute deviation of any cofactor atom in this area is ~1.5 Å.

agreement between the refined model and the data (Figure 3). For comparison, Figure 4 illustrates an omit–difference map of the 2.4.1 model around M202.

The change in the M202 side chain, the loss of magnesium from D_B, and the apparent loss of a water molecule are the most significant structural changes in the vicinity of the mutation evident at 3.0-Å resolution (Figure 5). Comparison of the final coordinates from multiple SA refinements of the 2.4.1 RC models starting from identical coordinates but differing in starting conditions (e.g., atomic dynamics velocities) suggests that the 2.4.1 RC coordinate accuracy is ~0.7 Å (A. J. Chirino and D. C. Rees, unpublished results), which compares reasonably well with the coordinate error (~0.5 Å) estimated by the method of Luzzati (1952). Overall, there was little change in the position of the special pair in this heterodimer, relative to the wild-type 2.4.1 structure, with the largest displacement in D_B being ~0.3 Å along the crystallographic *a* axis. Four nearby aromatic residues (Phe L181, Trp M185, Phe M189, and Phe M197) moved by as much as 1.3 Å. In both the 2.4.1 and M202HL structures, His L168 may be hydrogen-bonded either to the acetyl group of ring I of D_A or to residue L166. The overall RMS deviation of C_α atoms between the 2.4.1 and M202HL RCs is 0.7 Å (0.4 Å over C_α atoms from the 11 transmembrane α-helices). Excluding the mutation site, the largest differences between the two structures (>2.0 Å) occur almost exclusively in regions where electron density is poor, particularly in loop regions along the fringes of the protein.

L173HL crystals are 3–4 times smaller in volume than average native RC crystals and diffract to a Bragg spacing of 4.0 Å (Table 1). The highest peak ($+5.6\sigma$) in the protein region of the ($|F_o(2.4.1)| - |F_o(L173HL)|$) difference electron density map occurs between the replaced side chain and the center of the adjacent porphyrin ring (Figure 6). Two $+6\sigma$ peaks, which could not be interpreted, are also present in the solvent region of this map. An omit–electron density map calculated around L173 at a resolution of between 20.0 and 4.0 Å indicates that the L173 side chain is accurately positioned in the current 2.4.1 RC model (Figure 7). No positive difference density, indicating a water position, is observed between atoms Nδ1 of histidine L173 and OBD of $BChl_B$ in either this mutant difference map or native 2.4.1 ($|F_o| - |F_c|$) difference maps, even though a water molecule exists at this site in the *Rps. viridis* RC structure. Either the ability to detect a missing water molecule using difference Fourier map analysis is severely limited at 4.0-Å resolution, or a water molecule exists at this site in both native and mutant RCs.

Bacteriopheophytin-Modifying Mutant: Leu M214→His (M214LH). Diffraction data of the M214LH mutant were collected to 3.3-Å resolution. Difference Fourier maps were noisy around the mutation site and therefore were not as straightforward to interpret as in the heterodimer case. As a control, ($|F_o(M214LH)| - |F_c(2.4.1)|$) and ($|F_o(2.4.1)| - |F_c(2.4.1)|$) difference Fourier maps were calculated around Leu L185, the site related by the 2-fold symmetry axis to M214 that is close to BPh_B; these maps were relatively

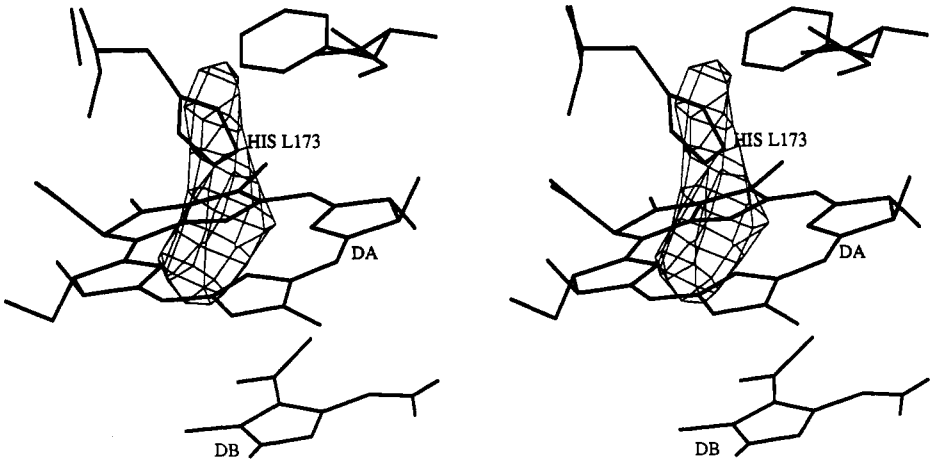

FIGURE 6: Stereo image of a difference Fourier map around the L173 site calculated using ($|F_o(2.4.1)| - |F_o(L173HL)|$) coefficients between 20- and 4.0-Å resolution and contoured at $+3.0\sigma$.

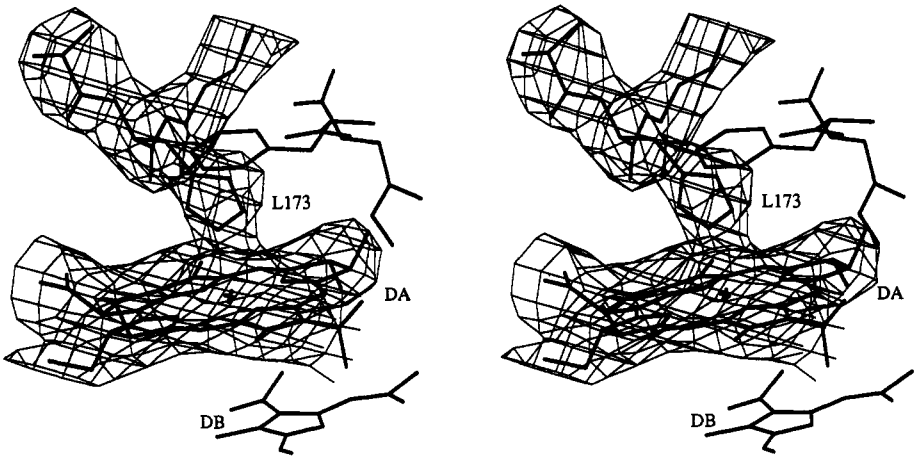

FIGURE 7: Stereo image of an ($|F_o(2.4.1)| - |F_c(2.4.1$, refined model)|) electron density map calculated between 20- and 4.0-Å resolution, within a 12 × 12 × 12 Å box around the L173 site (contoured at $+2.5\sigma$). Residues L172–L174 and D_A were omitted from the calculation of F_c. The view is roughly the same as that in Figure 6.

featureless (data not shown). Extra side-chain density at M214 was visible in the M214LH difference maps, such that the histidine imidazole ring could be positioned within ligand distance of a Mg in the porphyrin ring. No significant rigid body change in the overall position of BPh_A was indicated by the difference maps, although preliminary spectroscopic evidence suggests that the transition moments associated with the bacteriochlorophyll ring are rotated within the mutant protein (Schenck et al., 1993). The noise level surrounding the mutation site may reflect non-rigid body changes in the porphyrin ring orientation and/or the presence of multiple conformations with slightly different geometries, but these possibilities cannot be distinguished at the current resolution.

To quantitate the magnesium occupancy at the BPh_A site in the M214LH RC, difference electron density maps were calculated with coefficients ($|F_o(M214LH)| - |F_c|$) using reflections between 8.0- and 3.3-Å resolution, with the F_c calculated from a 2.4.1 wild-type RC model with the magnesium atoms of the four BChl groups removed. The electron density values of this map were scaled such that the average value was 0, with a standard deviation of 2 in arbitrary units. The magnesiums in the BChl were removed to serve as an internal standard to estimate the occupancy of Mg in the BPh groups. On this scale, the electron density values of the magnesium sites in the four BChl groups were observed to be 18, 36, 25, and 13 for $BChl_B$, D_B, D_A, and $BChl_A$, respectively. For comparison, when this calculation was repeated with the 2.4.1 wild-type RC data, the corresponding values were observed to be 26, 36, 26, and 11, respectively. Although the magnesiums in the BChl should all be fully occupied, and hence expected to have similar electron density values, the observed range of density values in these maps may reflect differences in positional disorder for the various Mg, differing displacements of the Mg from the center of the BChl rings, the effects of the limited resolution of the diffraction data, and/or the effects of errors in the structural model on the calculated structure factors. In the calculation with the M214HL data, the electron density values at the center of the BPh_A and BPh_B rings were 14 and 2, respectively, while the corresponding values for the 2.4.1 RC data were −2 and 2, respectively. Consequently, the electron density value (14) at the Mg site in the BPh_A group of the M214LH RC is within the range of values observed for the fully occupied BChl groups, while the BPh_B ring shows no evidence for Mg coordination (density value = 2). A more quantitative estimate of the Mg occupancy in the BPh_A site of the M214LH mutant is precluded by the uncertainties in this type of analysis, as evidenced by the range of density values observed for the magnesiums in the BChls. Biochemically, it appears that the Mg in the BPh_A site is fully occupied, as pigment extraction and metal binding studies suggest that one BPh has been replaced by one BChl in this mutant (Kirmaier et al., 1991).

Electron-Transfer Mutant: Tyr M210 → Phe (M210YF). Diffraction data were collected to 3.0 Å for the M210YF mutant (Table 1). Difference Fourier maps using coefficients ($|F_o(2.4.1)| - |F_o(M210YF)|$) failed to reveal significant differences in the mutant structure (except for the removal of the hydroxyl group at the M210 site). Examination of the

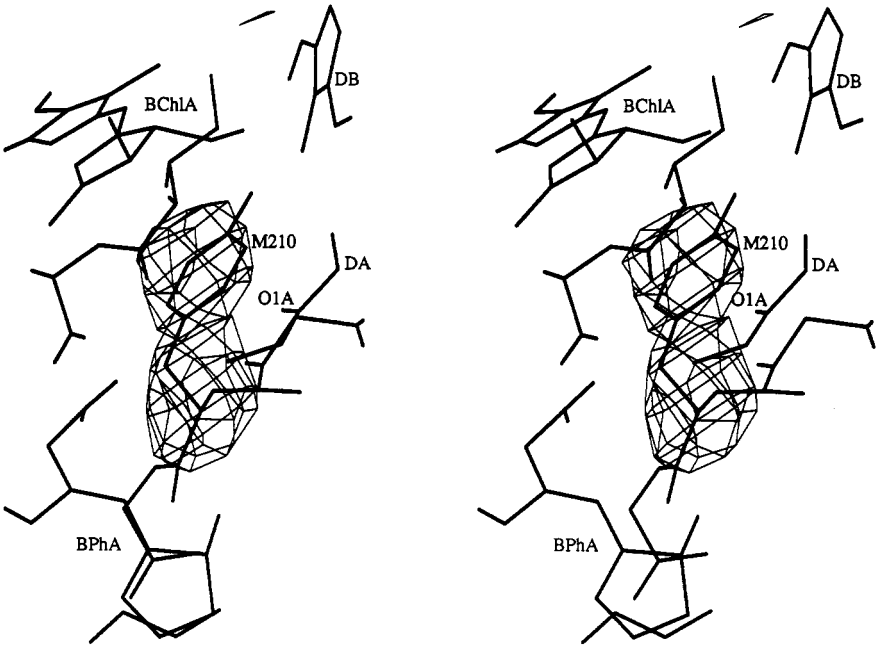

FIGURE 8: Stereo image of a difference Fourier electron density map calculated using ($|F_o$(M210YF)| − $|F_c$(2.4.1, refined model)|) coefficients after leaving out the M210 residue from the structure factor calculation. Reflections between 20- and 3.0-Å resolution were used, and the map was contoured at +3.0σ. Note that the phenylalanine difference density closely follows the tyrosine residue found in the wild-type structure.

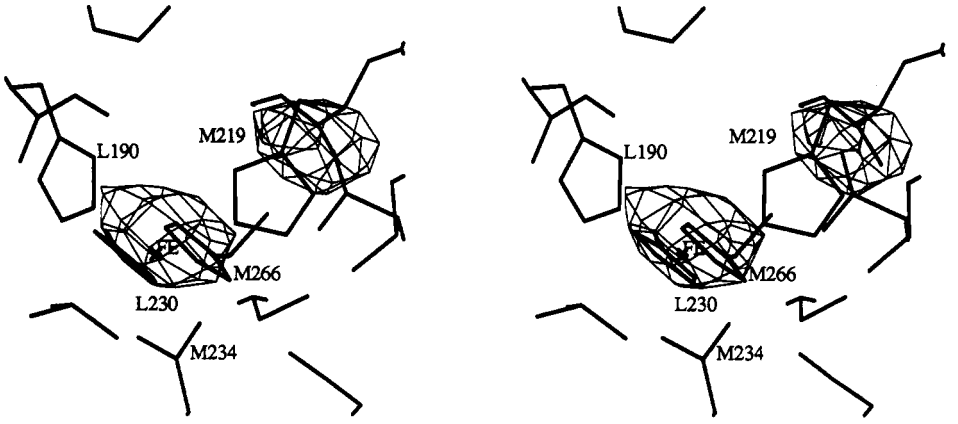

FIGURE 9: Stereo image of a difference Fourier electron density map calculated using ($|F_o$(2.4.1)| − $|F_o$(M219HC)|) coefficients between 20- and 4.0-Å resolution around the M219 site. The map is contoured at +3.0σ. The most prominent peaks are at the Fe site and residue M219.

($|F_o$(M210YF)| − $|F_c$(2.4.1)|) map with M210 removed from the structure factor calculation (Figure 8) demonstrates that the phenylalanine maintains a conformation similar to that of the wild-type tyrosine; no major secondary structure changes occur as a result of the mutation. This is in agreement with resonance Raman studies (Mattioli et al., 1991) and linear dichroism spectroscopy (Gray et al., 1990) of M210YF mutants, implying that the change in electron-transfer kinetics is due to the chemical difference between tyrosine and phenylalanine. This points to residue M210's involvement in fine tuning the energy levels of the charge-separated states relative to the D·BPh_A ground state, possibly via electrostatic interactions, which is in agreement with theoretical calculations (Parson et al., 1990) and experiment (Nagarajan et al., 1993).

The 2.4.1 RC coordinates with tyrosine M210 replaced by phenylalanine were refined against all reflections with $|F_o| > 0$ from the M210YF data set. Rigid body refinement using reflections between 8.0 and 5.0 Å (4753 reflections) produced little model movement, resulting in a negligible decrease in the R value (0.255–0.254). SA refinement using reflections between 8.0- and 3.0-Å resolution (18 370 reflections) reduced the R value to 0.218 [$|F| > 2\sigma_F$ (14 589 reflections), RMS_{bond} = 0.013 Å, and RMS_{angle} = 3.4°]. The overall RMS deviation of C_α atoms between 2.4.1 RC and M210YF is 0.7 Å (0.5 Å over C_α atoms from the 11 transmembrane α-helices).

Non-Heme Iron Mutant: His M219 → Cys (M219HC). Diffraction data for the M219HC mutant was collected to 4.0-Å resolution from crystals ~3–4 times smaller in volume than wild-type RC crystals and exhibited the largest change in unit cell dimensions of any of the mutants studied. ($|F_o$(2.4.1)| − $|F_o$(M219HC)|) difference Fourier maps (Figure 9) indicate that the largest positive difference peak (+6.4σ) in the crystallographic asymmetric unit is located at the iron site (consistent with the loss of Fe), while the second highest peak (+4.8σ) is located near residue M219. No major tertiary or quaternary structure rearrangements were indicated, although given the limited resolution and poor quality of the diffraction data (Table 1), few other details can be described. Site-directed mutagenesis has been performed on all of the other residues that form iron ligands, with the result that Fe is no longer present when any of the histidine ligands are altered although, in some cases, another transition metal (e.g., Zn or Mn) substitutes for Fe (J. C. Williams et al., manuscript

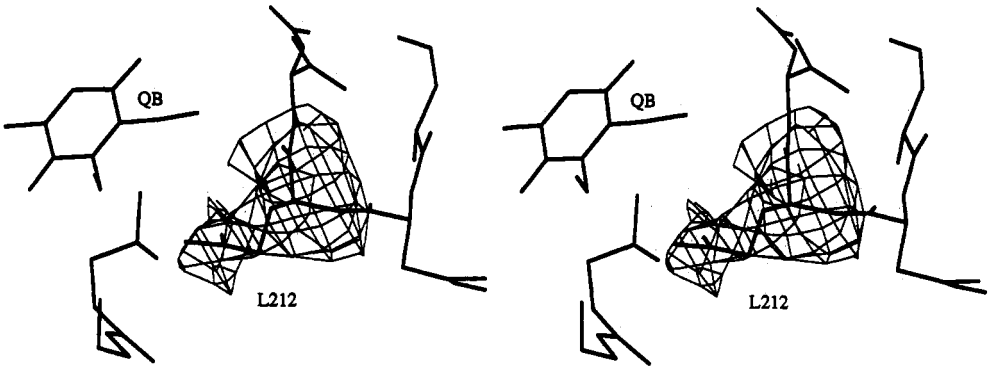

FIGURE 10: Stereo image of a difference Fourier electron density map calculated using ($|F_o$(L212EQ)| − $|F_c$(2.4.1, refined model)|) coefficients after leaving out residue L212 from the structure factor calculation. Reflections between 20- and 3.3-Å resolution were used, and the map was contoured at +2.5σ.

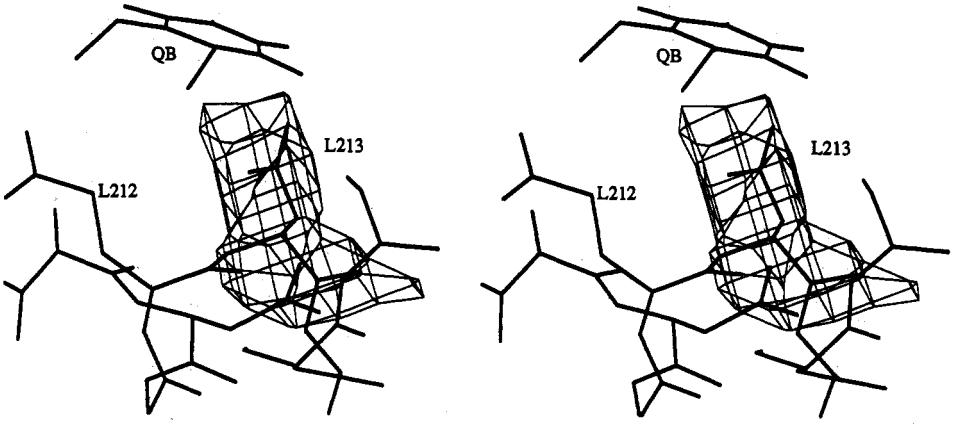

FIGURE 11: Stereo image of a difference Fourier electron density map calculated using ($|F_o$(L213DN))| − $|F_c$(2.4.1, refined model)|) coefficients after leaving out residue L213 from the structure factor calculation. Reflections between 20- and 3.3-Å resolution were used, and the map was contoured at +2.5σ. Several atoms were removed from this figure for clarity.

in preparation). While the presence of a divalent cation increases the electrostatic potential favoring electron transfer from Q_A to Q_B (Yeates et al., 1987), its presence is not mandatory since mutants with Fe-free RCs are capable of growing photosynthetically, albeit at slower rates (Williams et al., 1991; J. C. Williams et al., manuscript in preparation). Furthermore, since M219HC folds properly, the iron is not required for final RC assembly.[5] However, the mutant appears to be less stable than the native RC (J. C. Williams et al., manuscript in preparation). A possible role of the iron may be to organize and align the histidines and quinone sites for optimal electron-transfer kinetics.

Proton-Transfer Mutant: Glu L212 → Gln (L212EQ) and Asp L213 → Asn (L213DN). X-ray diffraction data were collected from L212EQ and L213DN crystals to 3.3- and 3.0-Å resolution, respectively. SA refinement of the L213DN structure using diffraction data between 8.0 and 3.0 Å (21 511 reflections) reduced the R value to 0.228 [$|F| > 2\sigma_F$ (19 413 reflections), RMS_{bond} = 0.013 Å, RMS_{angle} = 3.3°]. Examination of ($|F_o$(2.4.1)| − $|F_o$(mutant)|) difference maps as well as ($2|F_o| - |F_c|$) and ($|F_o| - |F_c|$) difference maps showed no significant movement of the Q_B ring, the L212 or L213 side chains (Figures 10 and 11), or the main chain. This implies that the change in proton uptake and electron-transfer kinetics (Okamura & Feher, 1992) associated with the substitution of these residues primarily reflects changes in the properties of the amino acid side chains.

[5] It is assumed that the composition of the isolated RC reflects the in vivo composition. This assumption can be tested by measuring the electron-transfer kinetics in chromatophores.

CONCLUSIONS

While the residue substitutions and corresponding cofactor alterations discussed in this work influence the functional behavior of the RC, none of these changes were associated with structural rearrangements of the protein visible at 3.0-Å resolution or lower. The similarities between the native and mutant structures suggest that the altered behavior of these mutants is primarily the result of differences in the chemical nature of the substituted side chains. The observation that many of these mutant RCs can support photosynthetic growth, even with a reduced quantum yield for charge separation, indicates an unexpected overall structural and functional robustness in the RC. Given the close to 100% quantum yield for electrons transferred in the forward direction in wild-type RCs, which so far has not been reproduced in model compounds, one might have expected that the RC function would be exquisitely sensitive to structural mutation. However, this does not seem to be true in these mutants, even in M219HC, in which the iron that was thought to play an important structural role is missing. The robustness of these mutants highlights the important problem of membrane protein stability and the energetic consequences of protein folding in a predominantly nonaqueous environment, where the contribution of hydrophobic interactions to stabilizing the tertiary structure of the RC should be less significant than for water-soluble globular proteins [see Rees et al. (1994) for a relevant discussion].

ACKNOWLEDGMENT

Use of the X-ray data collection facilities at UCLA and the

Cray YMP at the National Science Foundation-supported San Diego Supercomputer Center is gratefully acknowledged.

REFERENCES

Allen, J. P., Feher, G., Yeates, T. O., Rees, D. C., Deisenhofer, J., Michel, H., & Huber, R. (1986) *Proc. Natl. Acad. Sci. U.S.A. 83*, 8589–8593.

Allen, J. P., Feher, G., Yeates, T. O., Komiya, H., & Rees, D. C. (1987) *Proc. Natl. Acad. Sci. U.S.A. 84*, 5730–5734.

Allen, J. P., Feher, G., Yeates, T. O., Komiya, H., & Rees, D. C. (1988) *Proc. Natl. Acad. Sci. U.S.A. 85*, 8487–8491.

Allen, J. P., Lous, E. J., Feher, G., Chirino, A., Komiya, H., & Rees, D. C. (1990) in *Current Research in Photosynthesis* (Baltscheffsky, M., Ed.) pp 61–64, Kluwer, Dordrecht, The Netherlands.

Bernstein, F. C., Koetzle, T. F., Williams, G. J. B., Meyer, E. F., Brice, M. D., Rodgers, J. R., Kennard, O., Shimanouchi, T., & Tasumi, M. (1977) *J. Mol. Biol. 112*, 535–542.

Bethge, P. H. (1984) *J. Appl. Crystallogr. 17*, 215–215.

Brünger, A. T. (1992) *Nature 355*, 472–475.

Brünger, A. T., Kuriyan, J., & Karplus, M. (1987) *Science 235*, 458–460.

Brünger, A. T., Krukowski, A., & Erickson, J. W. (1990) *Acta Crystallogr. A46*, 585–593.

Bylina, E. J., & Youvan, D. C. (1988) *Proc. Natl. Acad. Sci. U.S.A. 85*, 7226–7230.

Chang, C.-H., El-Kabbani, O., Tiede, D., Norris, J., & Schiffer, M. (1991) *Biochemistry 30*, 5352–5360.

Chow, H. C., Serlin, R., & Strouse, C. E. (1975) *J. Am. Chem. Soc. 97*, 7230–7242.

Debus, R. J., Feher, G., & Okamura, M. Y. (1986) *Biochemistry 25*, 2276–2287.

Deisenhofer, J., Epp, O., Miki, K., Huber, R., & Michel, H. (1985) *Nature 318*, 618–624.

El-Kabbani, O., Chang, C.-H., Tiede, D., Norris, J., & Schiffer, M. (1991) *Biochemistry 30*, 5361–5369.

Ermler, U., Frtizsch, G., Buchanan, S., & Michel, H. (1992) in *Research in Photosynthesis* (Murata, N., Ed.) pp 341–347, Kluwer Academic Publishers, Amsterdam.

Farchaus, J. W., & Oesterhelt, D. (1989) *EMBO J. 8*, 47–54.

Feher, G. (1992) *J. Chem. Soc., Perkins Trans. 2 11*, 1861–1874.

Feher, G., Allen, J. P., Okamura, M. Y., & Rees, D. C. (1989) *Nature 339*, 111–116.

Finkele, U., Lauterwasser, C., Zinth, W., Gray, K. A., & Oesterhelt, D. (1990) *Biochemistry 29*, 8517–8521.

Gray, K. A., Farchaus, J. W., Wachtveitl, J., Breton, J., & Oesterhelt, D. (1990) *EMBO J. 9*, 2061–2070.

Hamlin, R. (1985) *Methods Enzymol. 114*, 416–452.

Hammes, S. L., Mazzola, L., Boxer, S. G., Gaul, D. F., & Schenck, C. C. (1990) *Proc. Natl. Acad. Sci. U.S.A.* **87**, 5682–5686.

Hanson, D. K., Nance, S. L., & Schiffer, M. (1992) *Photosynth. Res. 32*, 147–153.

Hanson, D. K., Tiede, D. M., Nance, S. L., Chang, C.-H., & Schiffer, M. (1993) *Proc. Natl. Acad. Sci. U.S.A. 90*, 8929–8933.

Howard, A. J., Nielsen, C., & Xuong, N. H. (1985) *Methods Enzymol. 114*, 452–472.

Howard, A. J., Gilliland, G. L., Finzel, B. C., Poulos, T. L., Ohlendorf, D. H., & Salemme, F. R. (1987) *J. Appl. Crystallogr. 20*, 383–387.

Jia, Y., DiMagno, T. D., Chan, C.-K., Wang, Z., Du, M., Hanson, D. K., Schiffer, M., Norris, J. R., Fleming, G. R., & Popov, M. S. (1993) *J. Phys. Chem. 97*, 13180–13191.

Jones, T. A. (1985) *Methods Enzymol. 115*, 157–171.

Kabsch, W. (1976) *Acta Crystallogr. A32*, 922–923.

Kirmaier, C., Holten, D., Bylina, E. J., & Youvan, D. C. (1988) *Proc. Natl. Acad. Sci. U.S.A. 85*, 7562–7566.

Kirmaier, C., Gaul, D., DeBey, R., Holten, D., & Schenck, C. C. (1991) *Science 251*, 922–927.

Komiya, H., Yeates, T. O., Rees, D. C., Allen, J. P., & Feher, G. (1988) *Proc. Natl. Acad. Sci. U.S.A. 85*, 9012–9016.

Laussermair, E., & Oesterhelt, D. (1992) *EMBO J. 11*, 777–783.

Luzzati, P. V. (1952) *Acta Crystallogr. 5*, 802–810.

Matthews, B. W., & Czerwinski, E. W. (1975) *Acta Crystallogr. A31*, 480–487.

Mattioli, T. A., Gray, K. A., Lutz, M., Oesterhelt, D., & Robert, B. (1991) *Biochemistry 30*, 1715–1722.

McDowell, L. M., Gaul, D., Kirmaier, C., Holten, D., & Schenck, C. C. (1991) *Biochemistry 30*, 8315–8322.

McPherson, P. H., Okamura, M. Y., & Feher, G. (1990a) *Biochim. Biophys. Acta 1016*, 289–292.

McPherson, P. H., Schonfeld, M., Paddock, M. L., Feher, G., & Okamura, M. Y. (1990b) *Biophys. J. 57*, 404.

Michel, H., Epp, O., & Deisenhofer, J. (1986) *EMBO J. 5*, 2445–2451.

Michel-Beyerle, M. E., Plato, M., Deisenhofer, J., Michel, H., Bixon, M., & Jortner, J. (1988) *Biochim. Biophys. Acta 932*, 52–70.

Nabedryk, E., Robles, S. J., Goldman, E., Youvan, D. C., & Breton, J. (1992) *Biochemistry 31*, 10852–10858.

Nagarajan, V., Parson, W. W., Gaul, D., & Schenck, C. C. (1990) *Proc. Natl. Acad. Sci. U.S.A. 87*, 7888–7892.

Nagarajan, V., Parson, W. W., Davis, D., & Schenck, C. C. (1993) *Biochemistry 32*, 12324–12336.

Okamura, M. Y., & Feher, G. (1992) *Annu. Rev. Biochem. 61*, 861–896.

Okamura, M. Y., Paddock, M. L., McPherson, P. H., Rongey, S., & Feher, G. (1992) in *Research in Photosynthesis* (Murata, N., Ed.) pp 349–356, Kluwer Academic Publishers, Amsterdam.

Paddock, M. L., Rongey, S. H., Feher, G., & Okamura, M. Y. (1989) *Proc. Natl. Acad. Sci. U.S.A. 86*, 6602–6606.

Parson, W. W., Chu, Z.-T., & Warshel, A. (1990) *Biochim. Biophys. Acta 1017*, 251, 272.

Reeke, G. N. (1984) *J. Appl. Crystallogr. 17*, 125–130.

Rees, D. C., Chirino, A. J., Kim, K.-H., & Komiya, H. (1994) in *Membrane Protein Structure: Experimental Approaches* (White, S. H., Ed.) Oxford Univ. Press, Oxford U.K. (in press).

Rongey, S. H., Paddock, M. L., Feher, G., & Okamura, M. Y. (1993) *Proc. Natl. Acad. Sci. U.S.A. 90*, 1325–1329.

Schenck, C., Corey, S., Kirmaier, C., & Holten, D. (1993) *Biophys. J. 64*, A18.

Takahashi, E., & Wraight, C. A. (1992) *Biochemistry 31*, 855–866.

Takahashi, E., Maroti, P., & Wraight, C. A. (1989) in *Current Research in Photosynthesis* (Beltscheffsky, M., Ed.) pp 169–172, Kluwer, Dordrecht, The Netherlands.

Treutlein, H., Schulten, K., Brünger, A. T., Karplus, M., Deisenhofer, J., & Michel, H. (1992) *Proc. Natl. Acad. Sci. U.S.A. 89*, 75–79.

Warshel, A., Chu, Z.-T., & Parson, W. W. (1989) *Science 246*, 112–116.

Williams, J. C., Paddock, M. L., Feher, G., & Allen, J. P. (1991) *Biophys. J. 59*, 142a.

Yang, S., & Jacobson, R. A. (1991) *Inorg. Chim. Acta 190*, 129–134.

Yeates, T. O., Komiya, H., Rees, D. C., Allen, J. P., & Feher, G. (1987) *Proc. Natl. Acad. Sci. U.S.A. 84*, 6438–6442.

Yeates, T. O., Komiya, H., Chirino, A., Rees, D. C., Allen, J. P., & Feher, G. (1988) *Proc. Natl. Acad. Sci. U.S.A. 85*, 7993–7997.

Yen, H.-C., & Marrs, B. (1977) *Arch. Biochem. Biophys. 181*, 411–418.

Youvan, D. C., Ismail, S., & Bylina, E. J. (1985) *Gene 38*, 19–30.